Characterizing a liquid crystal spatial light modulator at oblique incidence angles using the self-interference method

Zixin Zhao (赵自新)[1,*], Yiying Zhuang (庄义颖)[1], Zhaoxian Xiao (肖昭贤)[2], Hangying Zhang (张航瑛)[1], Chen Fan (樊 晨)[1], Hehui Geng (耿贺辉)[1], and Hong Zhao (赵 宏)[1]

[1]*State Key Laboratory for Manufacturing Systems Engineering, School of Mechanical Engineering, Xi'an Jiaotong University, Xi'an 710049, China*

[2]*Institute of Systems Engineering, China Academy of Engineering Physics, Mianyang 621000, China*

**Corresponding author: zixinzhao@xjtu.edu.cn*

Received April 9, 2018; accepted August 7, 2018; posted online August 31, 2018

The phase modulation characteristics of a reflective liquid crystal (LC) spatial light modulator (SLM) under oblique incidence are studied by using our proposed self-interference method. The experimental setup of the method is very simple and has good robustness to mechanical vibrations. By changing the gray value of the combined grayscale loaded on the LC-SLM, different sheared fringe patterns, generated by the interference between the constant phase-modulated beam and the +1-order diffracted beam of the blazed grating, can be obtained. The amount of phase modulation of the LC-SLM is obtained by subtracting the phase of the two side lobes in the frequency domain. By turning the turntable where the SLM is mounted, the phase modulation characteristics at different incident angles can be measured. The experimental results show that the phase modulation curves do not change significantly with the small angle. When the angle is large (i.e. larger than 10°), the phase modulation curves become different, especially for the high gray levels. With the increase of the incident angle, the phase modulation depth is reduced. The results indicate that the incident angle plays an important role in the performance of the phase modulation of an LC-SLM.

OCIS codes: 070.6120, 120.5060, 120.5050, 050.1950.

doi: 10.3788/COL201816.090701.

A liquid crystal (LC) spatial light modulator (SLM), based on the principle of electronically controlled birefringence of LC, can be used for modulating the amplitude and phase of light by changing the driving electric signal. Due to its advantages of low power consumption, no mechanical inertia, and programmable control, it is widely used in adaptive optics[1], diffractive optical elements[2], optical tweezers[3,4], optical metrology[5,6], and so on. As a key device in the modern optical field, its phase modulation characteristics need to be known and calibrated accurately.

Plenty of research has been conducted on the measurement of phase modulation characterization with different methods, which can be categorized into two groups: interferometry-based methods and diffraction-based methods. The interferometry-based methods mainly include Twyman–Green interferometry[7–9], Mach–Zehnder interferometry[10,11], and double-slit interferometry[12]. For the Twyman–Green and Mach–Zehnder interferometry-based methods, the reference beam and test beam travel in different ways before they interfere. As a result, these two methods are very sensitive to mechanical vibrations and air turbulence. The double-slit interferometry-based method can overcome the drawbacks to some extent, as the reference and test beams travel almost in the same way. Nevertheless, only a small part of the SLM can be calibrated because of the use of the double slit. The diffraction-based methods[13,14], by measuring the intensity of a single fixed diffraction order in the far field for differently shaped gratings on the SLM, have a high robustness to vibrations and air turbulence. The intensity image is characterized by the cosine of the effective phase difference, and the phase shift calculation needs a very sophisticated nonlinear optimization process.

It should be noted that Panezai *et al.*[12] have studied the oblique incidence characterization of an SLM by using double-hole interferometry and an image post-processing method. Nevertheless, it cannot be applied in the condition of normal incidence or oblique incidence with a quite small angle. Recently, Fuentes *et al.*[15] proposed an interferometric method using a self-generated diffraction grating. In their method, the configuration is quite simple, and the beam is incident at a small angle about the SLM plane, which is a suitable way to study the phase modulation characteristics under different incident angles. However, they calculated the phase shift through the executive two fringe patterns, where the environmental disturbance may influence the measuring accuracy. As a result, we propose an enhanced method, called the self-interference method, to calibrate the phase response of the SLM based on Fuentes's method[15]. In our proposed method, the grayscale pattern loaded on the SLM is improved. Specifically, the improved pattern consists of a blazed grating and two constant grayscale patterns so

that the phase shift can be calculated using only one interferogram.

In this Letter, the performance of a reflective LC-SLM under oblique incidence is studied based on the self-interference method. The experimental configuration is quite simple and robust. Based on the self-interference method, the phase modulation curves of the LC-SLM can be obtained under different angles of incidence with the help of Fourier phase analysis.

The working principle of an LC-SLM is based on the electronically controlled birefringence of the LC. As Fig. 1 shows, the nematic LC layer is sealed in a cavity several micrometers thick. Nematics are nanometer-sized, anisotropic LCs characterized as lacking positional order, but maintaining a high degree of orientational order[16]. When the beam is incident on the LC layer, it splits into two components, ordinary and extraordinary light, due to the ordinary refractive index n_o and extraordinary refractive index n_e of LC molecules. As an electric field is applied ($U \geq U_L$, a threshold voltage), as shown in Fig. 1(b), LC molecules will rotate through an angle α, and the angle φ ($\varphi = \frac{\pi}{2} - \alpha$) is the angle between the long axis of the LC molecules and the normal direction of the SLM plane. As a result, the extraordinary refractive index n_e that is dependent on the angle φ is called the effective extraordinary refractive index $n_e(\varphi)$ and can be determined according to Eq. (1)[17]:

$$\frac{1}{n_e^2(\varphi)} = \frac{\sin^2\varphi}{n_e^2} + \frac{\cos^2\varphi}{n_o^2}, \tag{1}$$

where n_e is considered the off-state extraordinary refractive index. When the light is incident on the LC-SLM, the refraction angle after the light that passes through the glass substrate is θ, $n_e(\varphi)$ can be replaced by $n_e(\varphi+\theta)$ and $n_e(\varphi-\theta)$ for the incident and reflected beams, respectively[17]. For the phase-only modulation of an SLM, the phase shift ξ_L caused by the change of gray level can be described as follows:

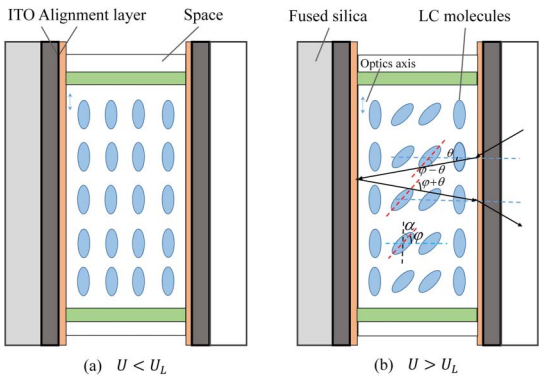

Fig. 1. Schematic diagram of LC-SLM. ITO, indium tin oxide.

$$\xi_L = \frac{2\pi d}{\lambda \cos\theta}[n_e(\varphi_L+\theta) - n_e(\varphi_0+\theta) + n_e(\varphi_L-\theta) - n_e(\varphi_0-\theta)], \tag{2}$$

where d is the thickness of the cavity, φ_L and φ_0 represent the angles between the long axis of the LC molecules and the normal direction of the SLM plane, which are caused by the electric field corresponding to the gray level L ($0 \leq L \leq 255$) and zero, respectively. It can be seen that the phase modulation characteristics under the oblique incidence condition are considered dependent on two parameters (φ, θ), since φ depends on the applied voltage determined by the gray level of the fringe pattern loaded on the SLM, whereas the refraction angle θ depends on the incident angle that can be experimentally adjusted. As a result, the incident angle plays an important role in the phase characterization of the LC-SLM.

The experimental setup of the self-interference method is shown in Fig. 2. A laser beam with a 532 nm wavelength is spatially filtered with the help of a microscopic objective and pinhole. It is then expanded into a collimated and polarized beam whose orientation is parallel to the direction of the LC molecule's axis for the sake of the phase-only modulation of the LC-SLM. The LC-SLM used in the experiment was made by Beijing RealLight Technology Co., Ltd., and the type is RL-SLM-RH. It has a target surface size of 12 mm × 7 mm and a resolution of 1920 pixel × 1080 pixel with a pixel pitch equal to 6 μm and a fill factor

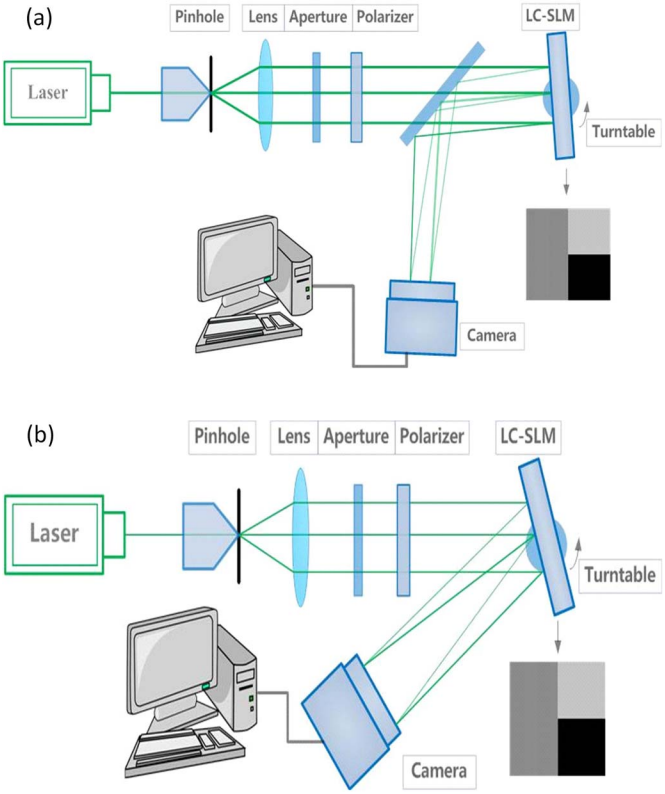

Fig. 2. Self-interference measurement system of LC-SLM under oblique incidence with (a) small incident angle and (b) large incident angle.

of 93%. To get a phase modulation curve under a quite small incident angle (i.e., less than 5°), a beam splitter was added into the configuration, as shown in Fig. 2(a). The experiment setup shown in Fig. 2(b) is suitable for characterizing the phase modulation under large incident angles.

The grayscale pattern loaded on the SLM is divided into three parts, as shown in Fig. 3. A blazed diffraction grating is loaded onto the left half of the screen, and the constant gray-level patterns are loaded onto the other half of the screen. Specifically, the zero gray-level pattern is loaded on the lower half of the screen and remains unchanged during the measurement process, while the gray value of the pattern loaded onto the upper half of the screen varies from 0 to 255. With the change of the gray value loaded on the upper half of the screen, a series of interference fringe patterns with different relative shifts between the upper and lower fringes can be captured by a complementary metal–oxide–semiconductor (CMOS) camera, as shown in Fig. 4(a). The phase modulation value can then be calculated using only one interferogram. As a result, our proposed self-interference method can reduce the effect of environmental vibrations or air turbulence.

A total of 33 inteferograms are recorded. Figure 4(a) shows one of the intensity maps captured by the CCD camera. Note that the distribution of the captured intensity map depends on where the CCD is placed. The longer the distance between the SLM plane and CCD plane, the more interference fringes can be captured by CCD. As the phase modulation value was estimated through the relative movement of the fringes, only the left sheared fringe pattern can be used. Besides, the right half of the pattern is the result of the diffraction in the sharp edge between the uniform grayscale zones. To reduce the influence of the diffraction, only part of the fringes, as shown in Fig. 4(b), was used to calculate the phase shift values. The phase demodulation from those interferograms is based on a fast Fourier transform (FFT) with a single line of data, and the phase modulation of the LC-SLM is calculated by subtracting the phase of the two side lobes in the frequency domain shown in Fig. 4(c). As shown in Fig. 4(b), the fringes passing through the red scan line represent the measuring area, and the fringes passing through the blue scan line represent the reference area. The blue line reference area can be expressed as

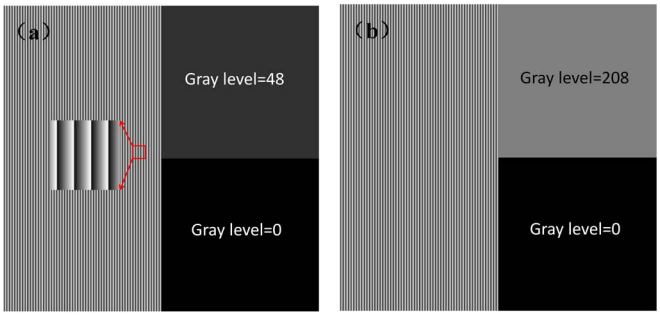

Fig. 3. Combined grayscale pattern loaded on the LC-SLM.

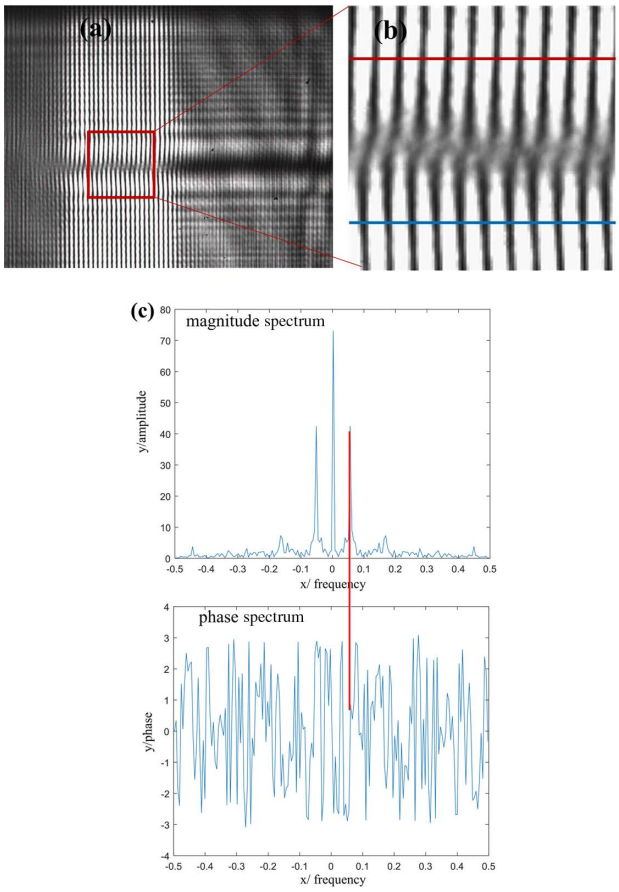

Fig. 4. Experimental results: (a) original fringe pattern, (b) extracted fringe pattern by red rectangle, (c) FFT result of one row.

$$i_1(x) = a(x) + b(x)\cos(2\pi f_{0x}x + \varphi_0), \tag{3}$$

where $a(x)$ is the background intensity, $b(x)$ is the modulation depth, f_{0x} is the spatial carrier frequency in the x direction, and φ_0 is the initial phase of the blue reference area fringe. The red line measurement area can be expressed as

$$i_2(x) = a(x) + b(x)\cos(2\pi f_{0x}x + \varphi_0 + \xi), \tag{4}$$

where ξ is the amount of phase shift between the measurement area and the reference area. The interference fringes given in Eqs. (3) and (4) are subjected to a continuous Fourier transform:

$$F(f) = \int_{-\infty}^{\infty} i(x)\exp(-2\pi jfx)\mathrm{d}x, \tag{5}$$

where $j = \sqrt{-1}$. Then, we can extract the first-order spectrum and obtain its inverse Fourier transform:

$$\begin{aligned} i_{11}(x) &= \int_{-\infty}^{\infty} F(f_{0x})\exp(2\pi jfx)\mathrm{d}f \\ &= c(x)\exp[j(2\pi f_{0x}x + \varphi_0)], \end{aligned} \tag{6}$$

$$i_{21}(x) = \int_{-\infty}^{\infty} F(f_{0x}) \exp(2\pi j f x) \mathrm{d}f = c(x) \exp[j(2\pi f_{0x} x + \varphi_0 + \xi)], \tag{7}$$

where

$$c(x) = \frac{1}{2} b(x), \tag{8}$$

and

$$2\pi f_{0x} x + \varphi_0 = \arctan \frac{\mathrm{Im}[i_{11}(x)]}{\mathrm{Re}[i_{11}(x)]}, \tag{9}$$

$$2\pi f_{0x} x + \varphi_0 + \xi = \arctan \frac{\mathrm{Im}[i_{21}(x)]}{\mathrm{Re}[i_{21}(x)]}. \tag{10}$$

Finally, the phase shift ξ is calculated by subtracting Eq. (10) from Eq. (9):

$$\xi = \arctan \frac{\mathrm{Im}[i_{21}(x)]}{\mathrm{Re}[i_{21}(x)]} - \arctan \frac{\mathrm{Im}[i_{11}(x)]}{\mathrm{Re}[i_{11}(x)]}. \tag{11}$$

In the actual calculation, 30 rows of data were used in one interferogram, and 15 phase modulation values can be obtained. The final phase shift result is the average of those 15 values.

To show the improvement of our proposed method over Fuentes' method, we have conducted eight experiments for normal incidence. The experiments were conducted four times using Fuentes' method and our proposed method, respectively. The results are shown in Fig. 5. Figure 5(a) shows four phase modulation curves using Fuentes' method, and Fig. 5(b) shows four phase modulation curves using our proposed method. It can be seen that the phase modulation curves obtained by our proposed method fluctuate much less than the curves obtained by Fuentes' method. Moreover, the maximum difference curves of each method were calculated and are shown in Fig. 5(c). Specifically, the root mean square (RMS) of the difference curves for Fuentes' and our proposed methods are 0.61 and 0.24 rad, respectively. As a result, our proposed method works more stably than Fuentes' method.

The LC-SLM was mounted on the rotation platform to precisely control the illumination angle. We first measured the phase modulation curve of the SLM under small incident angles using the configuration shown in Fig. 2(a). The phase characterization curves of the LC-SLM under oblique incidence as a function of the gray level are shown in Fig. 6(a). It can be seen that the phase modulation curves at different angles are almost coincident, which indicates that the influence of the incident angle on the phase modulation characteristics is not significant.

As can be seen from Fig. 6(b), the phase modulation values are nearly the same with a specific gray level (from 0 to 255) under different incident angles. The maximum phase shift, which is the phase modulation depth, is about

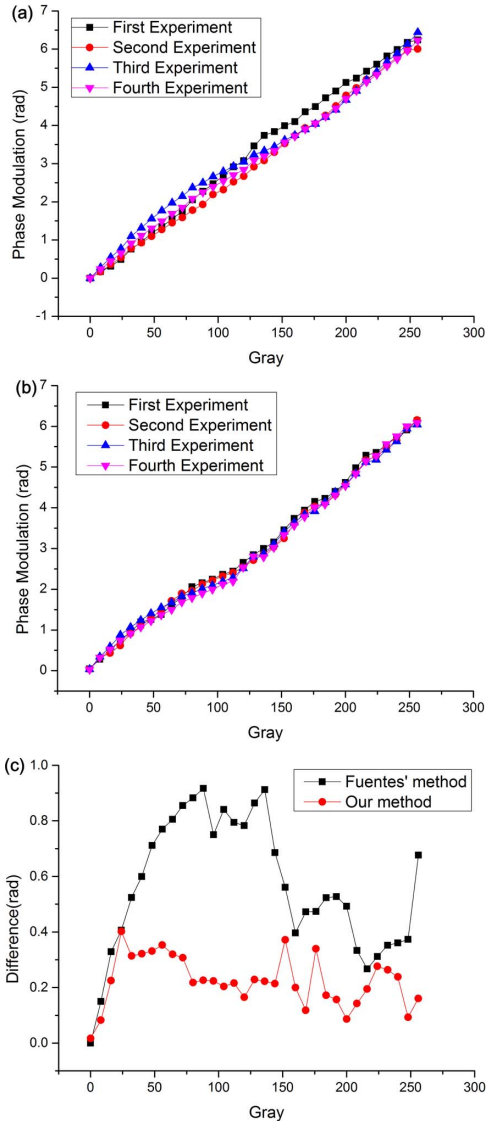

Fig. 5. Comparisons of our proposed method with Fuentes' method using data from eight experiments. (a) The four phase modulation curves were obtained using Fuentes' method; (b) the four curves were obtained using our proposed method; (c) the maximum phase difference curves of Fuentes' method (black squares) and our proposed method (red circles).

2π and remains almost unchanged with the change of the incident angle.

In addition, the phase modulation characteristic curves at the high incident angles (10°, 20°, 30°, 40°, 45°) are shown in Fig. 7(a). It can be seen that the trends of phase modulation under different incident angles are the same, and the value of phase modulation increases nonlinearly with the displayed gray level.

Moreover, the phase modulation decreases with the increase of the incident angle. Specifically, as shown in Fig. 7(b), the phase modulation values did not change much when the gray level was less than 200 but showed a great change when the gray level was over 200. Note that the phase modulation depth decreased from 6.3095 rad (normal incidence) to 4.5668 rad (oblique incidence

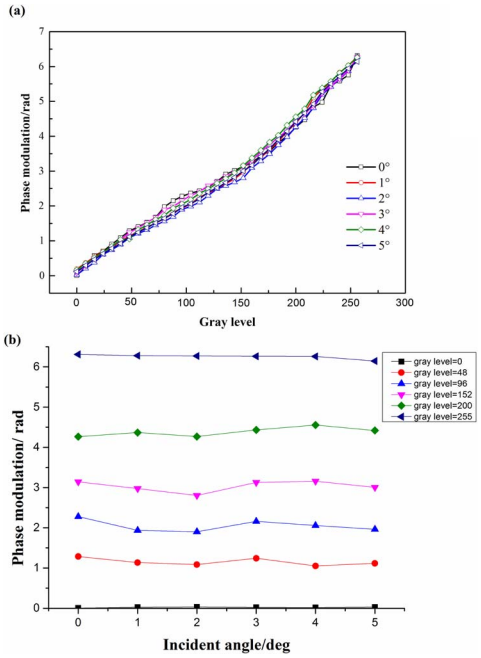

Fig. 6. Phase modulation properties of LC-SLM at small incident angles: (a) phase modulation curves for oblique illumination angles of 0°, 1°, 2°, 3°, 4°, 5°; (b) phase modulation values for specific gray levels (0, 48, 96, 152, 200, 255) under different incident angles.

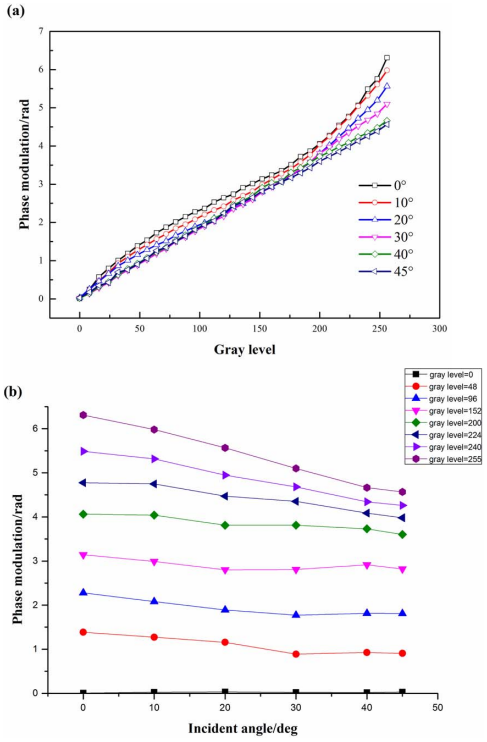

Fig. 7. Phase modulation properties of LC-SLM at large incident angles: (a) phase modulation curves for oblique illumination angles of 0°, 10°, 20°, 30°, 40°, 45°; (b) phase modulation values for specific gray levels (0, 48, 96, 152, 200, 224, 240, 255) under different incident angles.

of 45°), where the decrease was very significant. As a result, for a specific SLM, the oblique incidence illumination angle must be considered carefully for some applications where the phase modulation depth is concerned.

In this Letter, the phase modulation characteristics of a reflective LC-SLM under oblique incidence were studied by using the self-interference method. After loading a combined grayscale pattern on the LC-SLM, the phase modulation value could be calculated with only one interferogram using the FFT-based method. The experimental results showed that the phase modulation curves, as a function of the gray level, are almost coincident when the incident angle is small (i.e. less than 5°). While the incident angle is larger, the phase modulation curves become different, especially for high gray levels. With the increase of incident angle, the phase modulation depth decreases. This research contributes to the literature by designing a very simple experimental configuration and method to calibrate the phase response of an electrically addressed SLM.

This work was financially supported by the National Natural Science Foundation of China (No. 51705404), the China Postdoctoral Science Foundation (No. 2016M602806), and the Fundamental Research Funds for the Central Universities (No. xjj2017093).

References

1. B. Jiang, L. Chao, X. Li, M. Xia, Q. Mu, and Z. Cao, Opt. Express **17**, 10774 (2009).
2. I. Moreno, A. Lizana, A. Márquez, C. Iemmi, E. Fernández, J. Campos, and M. J. Yzuel, Opt. Express **16**, 16711 (2008).
3. A. Hermerschmidt, S. Krüger, T. Haist, S. Zwick, M. Warber, and W. Osten, Proc. SPIE **6905**, 690508 (2008).
4. G. Sinclair, J. Leach, P. Jordan, G. Gibson, E. Yao, Z. J. Laczik, M. J. Padgett, and J. Courtial, Opt. Express **12**, 1665 (2004).
5. E. Tajahuerce, J. Lancis, J. Ares, J. Arines, P. Prado, S. Bará, V. Climent, V. Durán, and Z. Jaroszewicz, Opt. Express **15**, 15287 (2007).
6. W. Osten, C. Kohler, J. Liesener, G. Krüger, W. Wernicke, D. Osten, N. Kayser, H. Demoli, and H. Gruber, Opt. Pur. y Apl. **38**, 71 (2005).
7. M. Yamauchi, A. Márquez, J. A. Davis, and D. J. Franich, Opt. Commun. **181**, 1 (2000).
8. H. Zhang, J. Zhang, and L. Wu, Meas. Sci. Technol. **18**, 1724 (2007).
9. S. Ma, D. Wang, Y. Wang, and L. Rong, Proc. SPIE **8913**, 89130M (2013).
10. X. Xun and R. W. Cohn, Appl. Opt. **43**, 6400 (2004).
11. S. Reichelt, Appl. Opt. **52**, 2610 (2013).
12. S. Panezai, D. Wang, J. Zhao, Y. Wang, L. Rong, and S. Ma, Opt. Eng. **54**, 037109 (2015).
13. O. Mendoza-Yero, G. Mínguez-Vega, L. Martínez-León, M. Carbonell-Leal, M. Fernández-Alonso, C. Doñate-Buendía, J. Pérez-Vizcaíno, and J. Lancis, J. Display Technol. **12**, 1027 (2016).
14. D. Engström, G. Milewski, J. Bengtsson, and S. Galt, Appl. Opt. **45**, 7195 (2006).
15. J. L. Fuentes, E. J. Fernández, P. M. Prieto, and P. Artal, Opt. Express **24**, 14159 (2016).
16. J. C. Gladish and D. D. Duncan, Opt. Eng. **55**, 054104 (2016).
17. L. C. Khoo, *Liquid Crystals* (Wiley, 2007).